s,p-d exchange interaction in Cr-based diluted magnetic semiconductors

W. Mac and A. Twardowski
Institute of Experimental Physics, Warsaw University, Warsaw, Poland

M. Demianiuk
Institute of Technical Physics, Military Academy of Technology, Warsaw, Poland

(Received 14 February 1996)

The *s,p-d* exchange interaction in Cr-based diluted magnetic semiconductors was studied by means of polarized magnetoreflectance and magnetization at $T=2$ K. The exchange constant $N_0\alpha - N_0\beta$ for four different zinc chalcogenides ($Zn_{1-x}Cr_xSe$, $Zn_{1-x}Cr_xSe_{0.95}S_{0.05}$, $Zn_{1-x}Cr_xS$, and $Zn_{1-x}Cr_xTe$) was determined. Assuming constant $N_0\alpha$ a chemical trend in $N_0\beta$ variation is discussed. [S0163-1829(96)05332-5]

I. INTRODUCTION

Diluted magnetic semiconductors (DMS's, also known as semimagnetic semiconductors) are semiconducting materials based on classical semiconductors, such as CdTe or ZnSe, in which a fraction of nonmagnetic cations is substituted by magnetic ions (typically Mn, Fe, or Co).[1] One of the most characteristic features of DMS's is the strong exchange interaction between delocalized band electrons (*s*- and *p*-type) and localized electrons (*d*-type) of magnetic ions. This interaction yields spectacular magnetooptical and magnetotransport effects (such as Faraday rotation and Zeeman splitting).[1]

For the conduction band the dominant contribution to the exchange interaction results from a direct exchange, originating from simultaneous jumps of conduction band *s*-type electrons and the magnetic ion *d*-type electrons between their original orbitals. We note that the conduction band wave functions are built of *s*-type orbitals of nonmagnetic cations and *s*-type orbitals of magnetic ions; however, a sizeable overlap of the *s* and *d* wave functions occurs only for the latter. The other contributions to *s-d* exchange (both direct and indirect) either vanish or are very small and can, therefore, be neglected.[2] The exchange integral for the considered *s-d* direct exchange is positive, which means that ferromagnetic (*F*) ordering of electron spins is preferred. For II-VI DMS's with Mn, Fe, and Co, the *s-d* exchange was indeed found to be positive and only weakly dependent on both magnetic ion and host lattice.[1]

For the valence band the situation is different. This band originates from the anion *p*-type orbitals, which means that the overlap between these orbitals and the magnetic (cation) *d* orbital is rather small (as compared to magnetic ion *s-d* overlap) and the direct exchange is expected to be negligible. The dominant contribution to the exchange in this case results from indirect, kinetic *p-d* exchange. This process involves virtual jumps of *p* electron to the *d* state and back or the *d* electron to the *p* valence band state and back. In order to give some ideas about *p-d* exchange, a simple one-electron argumentation can be applied to explain the observed sign of *p-d* exchange. In this approximation, the splitting of spin-up and spin-down *p* levels results from their hybridization with the spin-up and spin-down *d* orbitals of *t* symmetry.[3] Since spin-up and spin-down *t* orbitals are strongly split, due to correlation effects (which are absent for delocalized *p* orbitals), the final splitting of *p* orbitals depends critically on the relative energy position of *p* and *t* spin-up (t_+) and -down (t_-) orbitals. In the case of a Mn, Co, or Fe ion, *p* orbitals are located far above t_+ and below t_- orbitals, which yields antiferromagnetic (AF) splitting of *p* orbitals.[3] An essentially different situation may be expected for ions with a less than half filled *d* shell, such as Cr (d^4), V (d^3), or Ti (d^2). For these ions the correlation splitting of unoccupied t_+ and t_- orbitals is much smaller than for occupied t_+ and t_- orbitals. Consequently, unoccupied t_+ and t_- orbitals can be located above the top of the valence band, which may lead to the ferromagnetic *p-d* exchange. The ferromagnetic *p-d* exchange was observed for $Zn_{1-x}Cr_xSe$ (Ref. 4) and preliminary data are available for $Zn_{1-x}Cr_xS$ (Ref. 5) and $Zn_{1-x}Cr_xTe$ (Ref. 6).

The problem of *p-d* exchange in DMS's (in particular, with ions other than Mn) was recently analyzed by Blinowski and Kacman,[7] as well as by Bhattacharjee[8] and Mašek.[9] It follows from Refs. 7 and 10 that for Mn (d^5), Fe (d^6), and Co (d^7) the *p-d* exchange should be AF type, and ferromagnetic for Sc (d^1) and Ti (d^2). Moreover for all these ions the Hamiltonian describing *p-d* exchange is predicted in a simple isotropic Heisenberg-type form ($\mathcal{H}\sim \mathbf{s}\cdot\mathbf{S}$, where $\mathbf{s}$ and $\mathbf{S}$ are spin operators of *p* and *d* electrons, respectively). For the other ions the situation is more complicated and the sign (*F* or AF) of *p-d* exchange depends on the particular location of the *d*-levels relative to the top of the valence band. The form of the *p-d* Hamiltonian for these ions is also more complicated.[7,8]

In this work, we present the results of magnetoreflectance and magnetization measurements for four different chromium based II-VI DMS: $Zn_{1-x}Cr_xSe$, $Zn_{1-x}Cr_xSe_{0.95}S_{0.05}$, $Zn_{1-x}Cr_xS$, and $Zn_{1-x}Cr_xTe$. We determine the *p-d* exchange constants for these materials and analyze the chemical trend of the interaction strength.

The paper is organized as follows: in Sec. II, we recall the basic facts concerning exchange-induced band splitting. The experimental procedure is described in Sec. III. Section IV

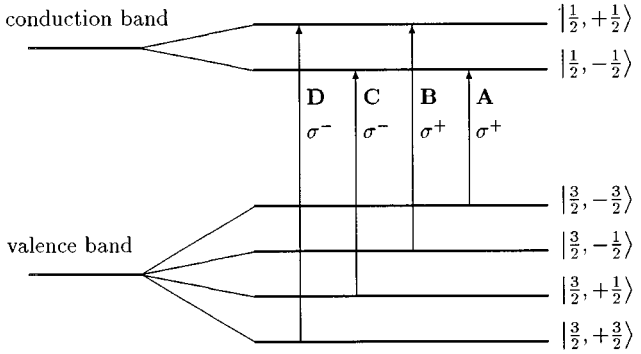

FIG. 1. Optical transitions between valence and conduction subbands visible in the Faraday configuration ($N_0\alpha>0$ and $N_0\beta<0$ were assumed).

presents the experimental results which are discussed in Sec. V.

II. THEORETICAL BACKGROUND

To describe the *p-d* (valence band–magnetic ion) and *s-d* (conduction band–magnetic ion) interaction in Mn-, Co-, and Fe-based DMS's the isotropic Heisenberg Hamiltonian was used. The mean field and virtual crystal approximations lead to the following form of the Hamiltonian:[1]

$$\mathcal{H}=-N_0 J x s_z\langle S_z\rangle, \tag{1}$$

where x is the magnetic ion concentration, J is the *p-d* or *s-d* exchange constant, $\langle S_z\rangle$ is the magnetic ion mean spin along the z axis, s_z is the z component of the band electron spin, and N_0 is the number of elementary cells in a unit volume. This Hamiltonian results in band splittings proportional to the mean spin of the magnetic ion. The valence band splits (in a magnetic field) into four subbands, which are equidistant if the exchange interaction constant for heavy and light holes is the same and the interaction between light holes and spin-orbit split holes is neglected. The conduction band splits into two components. Thus, there are eight possible optical transitions between the valence and the conduction band. Four of them are visible in the Faraday configuration (magnetic field parallel to the light wave vector) (Fig. 1). The energies of these transitions are described by the equations:

$$E_A=E_0+3b-3a, \quad E_B=E_0+b+3a,$$
$$E_C=E_0-b-3a, \quad E_D=E_0-3b+3a \tag{2}$$

where E_0 is the zero-field exciton energy, $a=(1/6)N_0\alpha x\langle -S_z\rangle$, $b=(1/6)N_0\beta x\langle -S_z\rangle$, α and β are exchange constants for the conduction and valence bands, respectively. The transitions A and B are allowed for circularly right polarized light (σ^+), while C and D are allowed for circularly left polarized light (σ^-). The four lines A, B, C, and D were clearly observed for several Mn-, Fe-, and Co-based DMS (for sufficiently large magnetic ion concentrations, $x>0.01$).[11,1] The lines A and D (resulting from the heavy hole exciton) are three times stronger than lines B and C.[11] Equation (2) takes into account only exchange-induced splitting. Usually, for large magnetic ion fractions x, the Zeeman splitting of a pure nonmagnetic crystal is much weaker than the exchange splitting and, in practice, may be neglected. However, for low x both must be considered.

The mean spin $\langle S_z\rangle$ of the magnetic ion may be obtained from the macroscopic magnetization M (per unit mass):

$$M=-\frac{x\mu_B\langle M_z\rangle}{m}, \tag{3}$$

where μ_B is the Bohr magneton. $M_z=L_z+2S_z$ is the z component of the magnetic moment operator, m is the mass of a single molecule. $\langle M_z\rangle=g\langle S_z\rangle$, where $g=2+\langle L_z\rangle/\langle S_z\rangle$, which leads to

$$M=-\frac{x\mu_B g\langle S_z\rangle}{m}. \tag{4}$$

The g factor may be obtained from model calculations. It was found that it is weakly magnetic field and temperature dependent for a typical magnetic field and temperature range.[12]

Equations (1), (2), and (4) allow one to determine the values of the exchange constants if the magnetization and exciton splitting are known. It follows from Eqs. (2) and (4) that

$$N_0(\alpha-\beta)=g\mu_B(E_D-E_A)/(Mm). \tag{5}$$

The integrals $N_0\alpha$ and $N_0\beta$ can be uncoupled using the energies of two other excitonic lines (E_B and E_C) and Eqs. (2). The other possibility is to evaluate $N_0\alpha$ from an independent experiment (e.g., Raman spin-flip experiment[13]).

III. EXPERIMENT

All the results presented in this paper were obtained for bulk crystals grown by the modified Bridgman technique from high purity ZnSe, ZnS, and ZnTe with pure metallic chromium. Single phase monocrystals were obtained only for rather low chromium concentrations, i.e., $x<0.007$ for $Zn_{1-x}Cr_xSe$, $Zn_{1-x}Cr_xSe_{0.95}S_{0.05}$, and $Zn_{1-x}Cr_xS$, but $x<0.001$ for $Zn_{1-x}Cr_xTe$. The chromium composition was checked by atomic absorption, electron microprobe, or wet chemical analysis. The low temperature magnetization and model calculations of single Cr^{2+} ion magnetic moment provided very accurate relative chromium concentration (for details see Ref. 12). Low temperature magnetization was also used to check the samples for the existence of chromium chalcogenides precipitations (ferromagnetic or ferrimagnetic). Only precipitation-free samples were used for the optical experiments. The crystalline structure was analyzed by a standard x-ray diffraction. The $Zn_{1-x}Cr_xSe$, $Zn_{1-x}Cr_xSe_{0.95}S_{0.05}$, and $Zn_{1-x}Cr_xTe$ revealed a zinc blende structure, while $Zn_{1-x}Cr_xS$ crystals were polytypes (mixed cubic and hexagonal structure).

In order to determine Zeeman band splitting, reflectance in the free exciton range was studied. The experiment was performed in the Faraday configuration for magnetic field up to 5 T. Samples were immersed in superfluid liquid helium at $T=2$ K. The light was reflected from the cleaved samples' (110) surfaces. Because of the strict selection rules in the Faraday configuration (Sec. II), the reflectance in two circular polarizations (σ^+ and σ^-) was measured. The polariza-

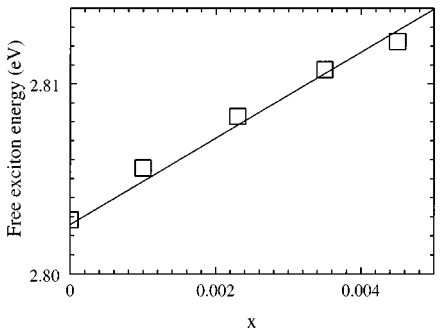

FIG. 2. The chromium concentration dependence of the free exciton line energy for $Zn_{1-x}Cr_xSe$ at $T=2$ K and $B=0$. The data points correspond to the center of the excitonic line, the total width of which was about 6 meV. x was determined from the low temperature magnetization (Ref. 12). The straight line corresponds to $E=(2.803+2.275x)$ eV.

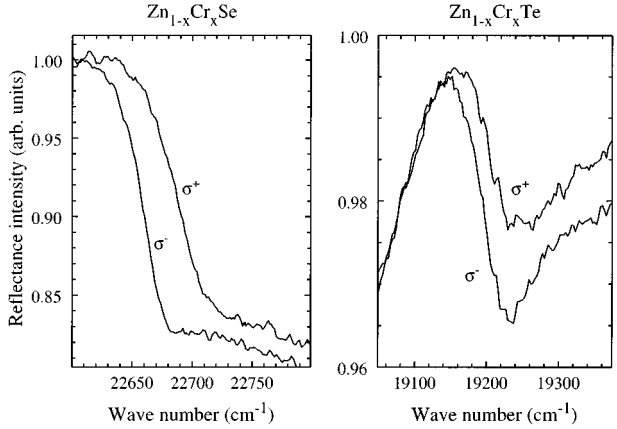

FIG. 3. Reflectance spectra in magnetic field $B=5$ T in circular polarizations σ^- and σ^+ for $Zn_{1-x}Cr_xSe$ and $Zn_{1-x}Cr_xTe$.

tion of the reflectance was analyzed using two different methods. In the first one, a standard setup with a photon counting system was used to record the σ^- and σ^+ spectra separately. In the second experiment, the difference between the intensities of two polarizations ($I_{\sigma^-}-I_{\sigma^+}$) was measured by a lock-in technique. Simultaneously, the total reflected signal ($I_{\sigma^-}+I_{\sigma^+}$) was recorded at a different frequency. For selected $Zn_{1-x}Cr_xSe$ and $Zn_{1-x}Cr_xTe$ samples both methods were applied and reasonable agreement was obtained.

The magnetization of the same samples, on which the magnetoreflectance measurements were performed, was measured using a superconducting quantum interference device (SQUID) magnetometer. The measurements were taken at $T=2$ K in a magnetic field up to 5 T for the same orientation as in the optical experiment.

IV. EXPERIMENTAL RESULTS

Steplike dispersive structures, typical for the free exciton, were observed in zero field reflectance spectra for all the studied crystals. The exciton energy was taken as the energy at which the excitonic structure attains half of its height. In the absence of a magnetic field, the exciton line shifts to higher energies with increasing chromium concentration. A reasonable linear behavior of exciton energy versus Cr concentration is observed for $Zn_{1-x}Cr_xSe$ (Fig. 2).

In the presence of a magnetic field, the reflectance spectra were recorded for two circular polarizations. Typical reflectance spectra for different compounds are presented in Fig. 3. A splitting of the excitonic structure in the magnetic field is clearly visible. However, due to low chromium concentration, the splitting, even in the strongest magnetic field (5 T), is smaller than the width of the structure. As a result, instead of four lines (A, B in σ^+ and C, D in σ^- polarization) only a single excitonic structure is visible in each polarization. We ascribe the structure in σ^+ to the mixture of A and B lines, and the structure in σ^- to the lines C and D. For all the investigated samples, the excitonic structure in the σ^+ circular polarization was blueshifted in respect to the structure in the σ^- polarization (Fig. 3). This is exactly the opposite to the behavior of all DMS's based on II-VI compounds with Mn, Co, and Fe,[1] and is compatible with ferromagnetic p-d exchange, as discussed below. As mentioned in Sec. II, for each polarization one of the lines (B for σ^+ or C for σ^-) is three times weaker than the other one (A or D). In view of that, the weak lines (B and C) are neglected and the structure in the σ^+ polarization is considered as corresponding to line A and in σ^- to line D. This rough assumption leads to an underestimation of the determined exciton splitting. This effect will be discussed below.

Following the above assumption, the exciton splitting $\Delta E \approx E_D - E_A$ was determined from the separately measured σ^+ and σ^- polarization spectra by subtracting the energy of excitons observed in the two polarizations. However, if the splitting is small compared to the structure width, ΔE can be determined with better accuracy using the directly measured difference between σ^+ and σ^- polarization spectra ($I_{\sigma^-}-I_{\sigma^+}$), as well as the total reflectance $R=I_{\sigma^-}+I_{\sigma^+}$ (where I is the intensity of the reflected light for σ^+ and σ^- polarizations, respectively). Calculating the degree of polarization,

$$\mathcal{P}=\frac{I_{\sigma^-}-I_{\sigma^+}}{I_{\sigma^-}+I_{\sigma^+}}, \tag{6}$$

and the logarithmic derivative of R over light energy E,

$$\mathcal{F}=\frac{\partial}{\partial E}\ln R, \tag{7}$$

one can obtain the splitting ΔE from the relation[14]

$$\mathcal{P}\simeq\frac{\Delta E}{2}\mathcal{F}. \tag{8}$$

Equation (8) holds if the shape of the reflectance structure is the same for both polarizations and if the splitting ΔE is reasonably smaller than the structure width. This procedure was used for $Zn_{1-x}Cr_xS$, $Zn_{1-x}Cr_xTe$ and some of the $Zn_{1-x}Cr_xSe$ samples. ΔE may be obtained from a comparison of $\mathcal{P}$ and $\mathcal{F}$ spectra in the entire spectral range. In practice, however, due to some reasons explained later, usually only the depths of the structures were compared. The examples of $\mathcal{P}$ and $(\Delta E/2)\mathcal{F}$ spectra are displayed in Fig. 4.

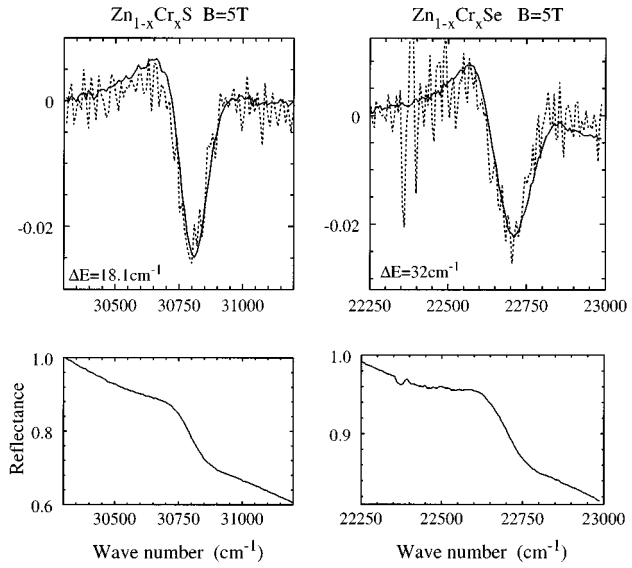

FIG. 4. The degree of polarization $\mathcal{P}$ spectra (solid line) together with the $(\Delta E/2)\mathcal{F}$ (dotted line) (a constant background was subtracted to provide the overlap of the spectra) and the total reflectance (R) for $Zn_{1-x}Cr_xSe$ and $Zn_{1-x}Cr_xS$.

We note that the dip observed for $\mathcal{P}$ spectra corresponds to $E(\sigma^+)>E(\sigma^-)$ [for $E(\sigma^+)<E(\sigma^-)$ a peak in $\mathcal{P}$ would be observed].

The exciton splitting (obtained using the procedures described above) as a function of magnetic field is exemplified in Fig. 5. The comparison of the two methods [i.e., the direct method and the one using the degree of polarization, Eq. (8)] performed for a few samples showed good agreement of the determined splittings. The experimental error of the data points in the Fig. 5 takes into account the following.

(1) If the splitting is very small and the excitonic structure is rather broad the degree of polarization $\mathcal{P}$ is low and becomes comparable to the polarization of the experimental setup, which is usually hard to reduce below a few percent. In our case, the setup polarization is caused mainly by the dichroism of the cryostat windows. In the simplest approxi-

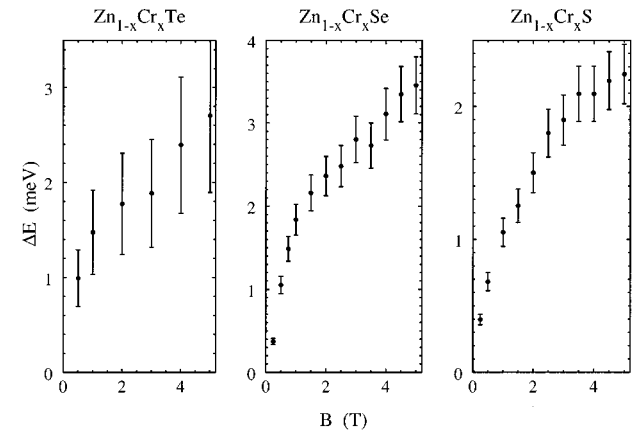

FIG. 5. The splitting of excitonic structure versus magnetic field for several samples of $Zn_{1-x}Cr_xSe$ ($x=0.0035$), $Zn_{1-x}Cr_xS$ ($x=0.0036$), and $Zn_{1-x}Cr_xTe$ ($x=0.0005$).

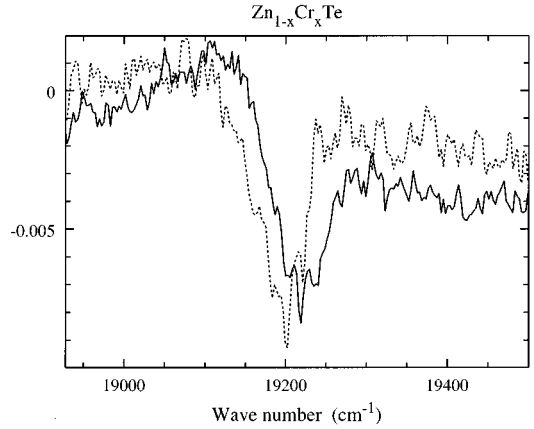

FIG. 6. The degree of polarization $\mathcal{P}$ spectrum (solid line) together with the $(\Delta E/2)\mathcal{F}$ spectrum (dotted line). A constant background was subtracted to provide the overlap of the spectra.

mation, the degree of polarization of the setup and the sample can be expressed as $\mathcal{P}=\mathcal{P}_{\text{setup}}+\mathcal{P}_{\text{sample}}$. In such a case, it is relatively easy to eliminate the setup contribution, because its energy dependence is much weaker than that of $\mathcal{P}_{\text{sample}}$. In practice, the linear interpolation of $\mathcal{P}$ from the outside of the excitonic structure was considered as $\mathcal{P}_{\text{setup}}$ and was subtracted from the measured $\mathcal{P}$.

(2) The other problem occurs when the derivative approximation [Eq. (8)] fails due to a relatively large splitting. In such a case, the shapes of $\mathcal{P}$ and $\mathcal{F}$ spectra are different. However, it appears that for splittings even as large as one third of the linewidth, the splitting determined from the ratio of $\mathcal{P}$ and $\mathcal{F}$ structure depths deviates from the real value by only a few percent (see the Appendix). For that reason, ΔE was obtained as a ratio of the depth of the dip in the $\mathcal{P}$ spectrum and the corresponding depth of the dip in $\mathcal{F}$.

(3) In some cases the shape of the excitonic structure in two polarizations is not the same (this is clearly visible for $Zn_{1-x}Cr_xTe$, see Fig. 3). The possible reason may be either asymmetric splitting [i.e., different from that described by Eq. (2)] of weak excitons B and C [which is, for instance, the case of pure ZnTe (Ref. 15)], or the different shape of the lines A and D. The difference i σ^+, σ^- spectra results in smaller accuracy of the determined splitting. For details see the Appendix.

Except for the problems discussed above, both methods determine the splitting of the ''mean'' exciton (mixed A and B or D and C), not the real difference: E_D-E_A. To estimate the systematic error introduced in this way it was assumed that the excitonic structure in each polarization is composed of two lines of different strength, but the same shape and energies described by Eq. (2). It follows from the model calculations presented in the Appendix that the determined splitting corresponds to the weighted average of the splittings of the strong (E_D-E_A) and weak (E_C-E_B) components [Eq. (A1)]. The knowledge of the relative behavior of the strong and weak excitons [Eq. (2) and $N_0\alpha$] allows one to obtain E_D-E_A from such an average. It will be argued later that it is reasonable to assume the $N_0\alpha$ exchange constant as 0.2 eV. Using this value one obtains that the real E_D-E_A splitting in the present case is from 10 to 20 % (depending on $N_0\beta$ magnitude) larger than the average

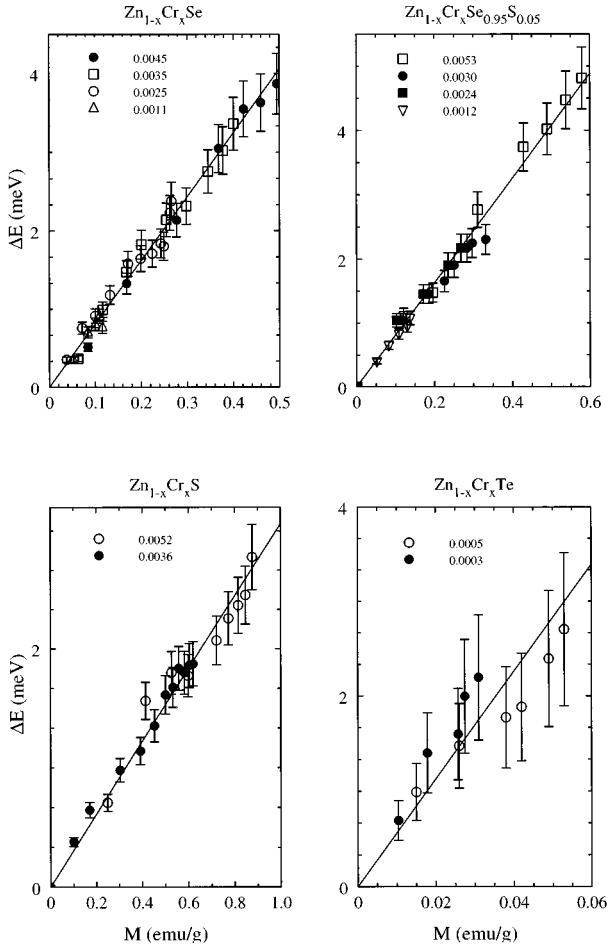

FIG. 7. The exchange exciton splitting (see text) versus magnetization (lattice diamagnetism corrected) for (a) $Zn_{1-x}Cr_xSe$, (b) $Zn_{1-x}Cr_xSe_{0.95}S_{0.05}$, (c) $Zn_{1-x}Cr_xS$, and (d) $Zn_{1-x}Cr_xTe$. Solid lines represents a linear fit of $\Delta E = aM$ to the data. The numbers in the plots indicate chromium concentration x as determined from magnetization measurements.

''mean'' exciton splitting. However, to avoid arbitrary assumptions and present the data as clearly as possible, this correction will be used only for the final result.

We note that for $Zn_{1-x}Cr_xTe$ the excitonic structures were much weaker than for the other compounds. Moreover, a significant difference between the shapes of the excitonic structure observed in two different polarizations shifts the $\mathcal{P}$ spectrum to higher energies with respect to the $\mathcal{F}$ spectrum and also makes it more asymmetric than it was for $Zn_{1-x}Cr_xSe$ or $Zn_{1-x}Cr_xS$ (Fig. 6). As a result, a lower accuracy of exciton splitting for $Zn_{1-x}Cr_xTe$ was obtained (Fig. 5).

Although the splitting of electronic bands in DMS's is usually dominated by the exchange interaction between magnetic ions and band electrons, for very small Cr concentrations the direct effect of the magnetic field on band electrons (Zeeman splitting in a pure, nonmagnetic crystal) may play an important role. To extract only the exchange-induced splitting, the exciton splitting for a nonmagnetic crystal was subtracted from the value obtained for the DMS crystal. The pure host lattice splitting was evaluated using the degree of polarization technique [Eq. (8)]. For ZnSe, ZnS, and ZnTe,

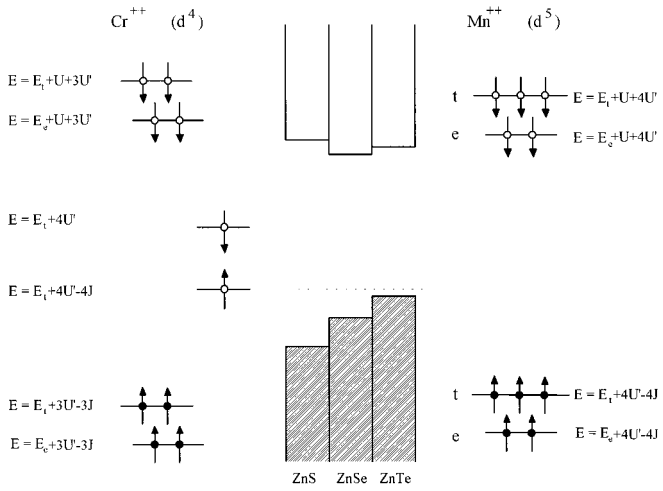

FIG. 8. Schematic diagram of relative position of ZnS, ZnSe, and ZnTe valence band and one one-electron [''U,U',J'' model of Kanamori (Ref. 21)] energy levels of Cr^{++} and Mn^{++}.

the σ^+ line was blueshifted with respect to the σ^- component. For ZnS a linear variation of exciton splitting with magnetic field was found with the slope 0.6 cm^{-1}/T. For ZnSe, 0.15 cm^{-1}/T was obtained while for ZnTe, 0.4 cm^{-1}/T. The observed splittings are in agreement with the results of other authors.[15]

In view of Eq. (5), the value of the exchange splitting $E_D - E_A$ (the total splitting corrected for pure host crystal Zeeman splitting) was compared to the magnetization measured for the same samples. The magnetization was corrected for the diamagnetic susceptibility of the host lattice [$\chi_d^{\mathrm{ZnSe}} = -3.2$ emu/g, $\chi_d^{\mathrm{ZnS}} = -3.9$ emu/g, and $\chi_d^{\mathrm{ZnTe}} = -3.0$ emu/g (Ref. 16)]. For all the studied $Zn_{1-x}Cr_xSe$, $Zn_{1-x}Cr_xSe_{0.95}S_{0.05}$, and $Zn_{1-x}Cr_xS$ samples a linear behavior of the exciton splitting versus magnetization (Fig. 7) was found. We stress that for the investigated samples the slope of the ΔE versus M seems to be concentration independent. The relatively large experimental error for $Zn_{1-x}Cr_xTe$ makes it difficult to conclude that the dependence of ΔE on M is both linear and concentration independent. In addition, the slope of the data for two $Zn_{1-x}Cr_xTe$ samples seems to differ slightly, although the difference is still within the experimental error. Such a small deviation may be caused by a slight inhomogeneity of the samples (magnetization probes the entire volume of the sample, while the reflectance comes from only a thin surface layer). On the other hand, an apparent concentration dependence of the p-d exchange has been observed, e.g., for $Cd_{1-x}Mn_xS$ (Ref. 17) and explained by multiple scattering effects.[18] However, the accuracy of the present experiment does not allow to formulate any pertinent conclusions.

The linear variation of the exciton splitting versus magnetization observed for $Zn_{1-x}Cr_xSe$ and $Zn_{1-x}Cr_xS$ strongly suggests that the exchange interaction may be described by a simple Heisenberg-type Hamiltonian. Equation (5) was used to fit the data and obtain the difference of exchange constants $N_0\alpha - N_0\beta$ for all the materials (Table I). The extraction of the p-d exchange constant ($N_0\beta$ parameter) requires the information about $N_0\alpha$, which is currently

TABLE I. Exchange constants (see text for details).

Material	$N_0(\alpha-\beta)$	$N_0\beta$	$N_0\beta$ (corrected)
$Zn_{1-x}Cr_xS$	-0.37 ± 0.1 eV	$+0.57\pm0.1$ eV	$+0.62$ eV
$Zn_{1-x}Cr_xSe_{0.95}S_{0.05}$	-0.63 ± 0.1 eV	$+0.83\pm0.1$ eV	$+0.93$ eV
$Zn_{1-x}Cr_xSe$	-0.65 ± 0.1 eV	$+0.85\pm0.1$ eV	$+0.95$ eV
$Zn_{1-x}Cr_xTe$	-3.4 ± 1.2 eV	$+3.6\pm1.2$ eV	$+4.25$ eV

not available for the investigated crystals. However, for the conduction band electrons, the s-d exchange interaction ($N_0\alpha$ parameter) is dominated by the direct exchange and hardly depends on the host crystal and magnetic ion. For all Mn-, Fe-, or Co-based II-VI DMS's known so far, $N_0\alpha$ is 0.2–0.25 eV.[1] Moreover, very recently the s-d exchange constant was evaluated from Raman spin-flip scattering for $Cd_{1-x}Cr_xS$ and a similar value of $N_0\alpha=0.22$ eV was obtained.[19] In view of that, $N_0\alpha=0.2$ eV was assumed for all our crystals. The p-d exchange constants ($N_0\beta$) resulting from this assumption are listed in Table I. The $N_0\beta$ values thus obtained are underestimated, since the weak components (B and C) were neglected as discussed above. If one assumes that the measured exciton splitting is the weighted average of the weak (B, C) and strong (A, D) exciton lines (cf. the Appendix) and adopts $N_0\alpha=0.2$ eV, then $N_0\beta$ values 10–20 % larger than the base results are obtained (last column of Table I).

V. DISCUSSION AND CONCLUSIONS

The evaluated p-d constants reveal ferromagnetic coupling between a Cr ion and the valence band electrons for the entire series of crystals, from ZnS to ZnTe. Moreover, the observed chemical trend of increasing magnitude of $N_0\beta$ from ZnS to ZnTe is exactly opposite to what was found for Mn-, Fe-, or Co-based DMS's (Ref. 1) and what was ascribed to increasing overlap of the wave functions with decreasing lattice constant. In the present case, the role of the energy position of the d level relative to the top of the valence band seems to be crucial for both the sign and the variation of $N_0\beta$. The model Hamiltonian commonly used for the description of p-d hybridization problem consists of three terms:

$$H=H_p+H_d+H_{\rm hyb}, \tag{9}$$

where H_p is the effective mass Hamiltonian for the valence band, H_d characterizes strongly interacting, atomiclike d states, and $H_{\rm hyb}$ describes p-d interaction between valence band and d states. The application of Hamiltonian (9) to DMS's has been discussed by several authors: Larson *et al.*,[20] Bhattacharjee,[8] Mašek[9] and most recently and completely by Blinowski *et al.*[7] For most semiempirical studies of Mn-DMS's, Hamiltonian (9) was represented by generalized Anderson Hamiltonian.[20] In this treatment, H_d was conveniently described by the so called ''U,U',J'' model of Kanamori.[21] We recall that in this model multielectron interaction is taken into account by introducing three parameters: U, which is the energy penalty for accommodating an additional electron on the orbital already occupied by another electron (with antiparallel spin), U' reflects the repulsive energy for two electrons on different orbitals (with any spins), and J is the energy gain if there is another electron on different orbital but with the spin parallel to the spin of the considered electron. Usually relation $U\gg U'\gg J$ holds. Kanamori model results in one-electron d orbitals (of t or e symmetry), which can be populated by a suitable number of electrons. The energies of the orbitals crucially depend (through U, U', and J parameters) on the number of electrons and their configuration. In particular, for the d^5 configuration (Mn^{2+}) the energy structure is relatively simple (Fig. 8): all the spin-up orbitals are populated, while all the spin-down orbitals are empty. Correlation effects lead to the spin-up–spin-down energy splitting equal $U+4J$. For the d^4 configuration (Cr^{2+}), the situation is essentially different (Fig. 8). Since one t spin-up orbital (t_+) is empty, its energy is higher by $U'-J$ than the energy of the populated t_+ orbitals. The correlation splitting for the unoccupied t orbitals is strongly reduced [$E(t_-)-E(t_+)=4J$, (Fig. 8)].

The p-d exchange splitting of the valence band states results from the hybridization with the d states. For the sym-

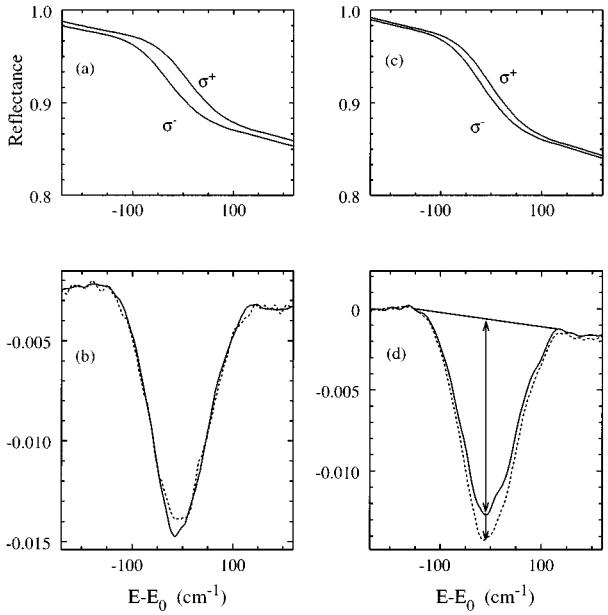

FIG. 9. (a) Simulation of spectra for two circular polarizations composed of A and D excitonic lines split by $\Delta E=40$ cm^{-1}. (b) $\mathcal{P}$ (solid line) and $(\Delta E/2)\mathcal{F}$ (dashed line) calculated for the above spectra. (c) Similar to (a), but with four excitonic lines A, B, C, and D, B, and C lines are three times weaker than A and D. (d) $\mathcal{P}$ (solid line) and $(\Delta E_{\rm strong}/2)\mathcal{F}$ (dashed line) for spectra from (c). For all spectra the real zero-field spectrum of $Zn_{1-x}Cr_xS$ was taken as a base. E_0 is the exciton energy at $B=0$. Arrows indicate the depths of the structures. See text for details.

metry reason, at the Γ point of the Brillouin zone, only t-type orbitals hybridize with the p-type states. Within the lines of the one-electron model, the effect of hybridization can be regarded as the repelling of the levels with the same spin.[3] Therefore in the case of Mn^{2+} t_+ levels, which are well below the top of the valence band (3–4 eV) will repel p_+ states upward, while the t_- levels, being above the top of the valence band, will pull p_- states downward. Effectively the valence band is split in the antiferromagnetic way ($\beta<0$). For Cr^{2+} situation is more complex due to empty t_+ and t_- orbitals, which may be close to the top of the valence band, and therefore may be decisive for the final splitting of the valence band. In particular, if t_+ orbital is above the top of the valence band, as depicted in Fig. 8, one could expect that the resulting downward repelling of p_+ will dominate other effects and the final splitting of the valence band will be ferromagnetic ($\beta>0$). Moreover the closer the empty t_+ orbital is to the top of the valence band, the stronger the splitting should be, which is equivalent to the larger magnitude of $N_0\beta$. Therefore, the observed ferromagnetic $N_0\beta$ for Cr-based DMS's could be interpreted as resulting from above the top of the valence band location of the empty t_+ orbital, while the populated t_+ orbitals are well below the top of the valence band. Taking into account the valence band offsets for ZnS, ZnSe, and ZnTe (Fig. 8) and the host lattice independence of transition metal ions levels location relatively affinity,[22] one should also expect the largest $N_0\beta$ value for $Zn_{1-x}Cr_xTe$, for which the energy denominator is the smallest. All of these predictions recover the experimental findings very well. One should be, however, aware of extending predictions of the one-electron model too far, since in some cases it may lead to false conclusions (although it predicts correctly the sign of $N_0\beta$ for Mn-, Co-, and Fe-based DMS's).

A much better model, taking into account multielectron effects in a more complete way, was recently developed by Blinowski *et al.*[7,10] This model properly recovers AF valence band splitting for Mn-, Fe-, and Co-DMS's and predicts the possibility of F p-d exchange for the Cr-based DMS's. The essential finding of this model is that the sign of the p-d exchange is governed mainly by the energy of the charge transfer from the Cr^{2+} (d^4) ion to the valence band (energy e_1 of Ref. 10). If this energy is positive, $N_0\beta$ should be negative, otherwise $N_0\beta$ is positive (i.e., ferromagnetic). The values of e_1 and e_2 (the charge transfer energy from the valence band to the Cr^{2+} ion) estimated from the donor energies for $Zn_{1-x}Cr_xS$ and $Zn_{1-x}Cr_xSe$ leads to $N_0\beta$ values surprisingly close to the experimental data.[10] For $Zn_{1-x}Cr_xTe$, e_1 is around zero and the result of the calculations was not clear. Having in mind the actual $N_0\beta$ value for $Zn_{1-x}Cr_xTe$, we should conclude that e_1 for this material is still negative, but its magnitude is smaller than for ZnS and ZnSe, which yields the largest $N_0\beta$.

It is worthwhile to note that the conditions for ferromagnetic p-d exchange derived from one-electron model of Kanamori[21] and many-electron model of Blinowski *et al.*[10] are compatible. The empty t_+ orbital located above the top of the valence band, which is equivalent to the relation $E_t+4U'-4J>E_p$, provides that also e_1 energy, calculated as the difference between energy of d^4 configuration ($=2E_t+2E_e+12U'-12J$) and the energy of d^3 configuration with one electron in the valence band ($=E_t+2E_e+6U'-6J+E_p$) is negative (since it is smaller than $-2U'+2J$). Therefore, in the case of the Cr-DMS's the one-electron model, although principally unjustified, leads to correct conclusions.

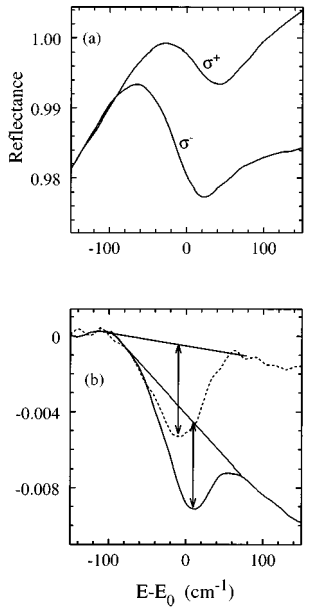

FIG. 10. Simulation of σ^+ and σ^- spectra for $Zn_{1-x}Cr_xTe$ with four excitonic components. Lines C and D are 1.5 times stronger than A and B, $\Delta E=30$ cm^{-1}. (b) $\mathcal{P}$ (solid line) and $(\Delta E/2)\mathcal{F}$ (dashed line) for the above spectra. E_0 is the exciton energy at $B=0$. Arrows indicate the depths of the structures. (See text for details.)

ACKNOWLEDGMENTS

The authors would like to thank Professor J. Blinowski and Professor J.A. Gaj for helpful discussions. This work was partially supported by the Committee for Scientific Research Grant No. 2P30B07009. One of us (W.M.) acknowledges the scholarship of Foundation for Polish Science.

APPENDIX: MODEL CALCULATIONS OF REFLECTANCE SPECTRA

Model calculations were performed to estimate the accuracy of the methods used in Sec. IV to determine the exciton splitting. In these calculations the excitonic spectrum was modeled by the smoothed, real zero field spectrum. The spectra for σ^+ or σ^- polarizations (in applied magnetic field) were constructed by shifting the basic excitonic line to an adequate energy [Fig. 9(a)], and if two lines (e.g., A and B) in one polarization were desired, the algebraic sum of two basic shapes was used [Fig. 9(b)].

(A) To check the applicability of the polarization degree method for large splittings only one line in each polarization was used (weak B and C lines were neglected). The lines were shifted in energy with respect to one another by ΔE. Then the $\mathcal{P}$ and $\mathcal{F}$ spectra were calculated. An example of such calculations for the highest experimental splitting $\Delta E=40$ cm^{-1} is presented in Fig. 9(b), where the $\mathcal{F}$ spec-

trum is multiplied by $\Delta E/2 = 20\ \mathrm{cm}^{-1}$. The $\mathcal{P}$ and $\mathcal{F}$ spectra do not match exactly, which reflects the inaccuracy of the method for such large ΔE. In the present case, ΔE determined from the depths of $\mathcal{P}$ and $\mathcal{F}$ is overestimated by about 6%. This overestimation decreases for smaller splittings. Similar calculations were also performed for the $Zn_{1-x}Cr_xTe$ line shape as well as for some other (e.g., sinusoidal) line shapes. For all of them, the overestimation of determined splitting was less than 6% if only the splitting was less than 0.2 of the linewidth.

(B) Next, the influence of weak components (lines *B* and *C*) on the determined splitting was studied. The lines *B* and *C* were taken to be three times weaker than the *A* and *D* lines, according to the expected intensity ratio of these lines (see Sec. II). The σ^+ and σ^- spectra obtained this way are exemplified for $\Delta E_{\mathrm{strong}} = 40\ \mathrm{cm}^{-1}$ and $\Delta E_{\mathrm{weak}} = 20\ \mathrm{cm}^{-1}$ in Fig. 9(c). In such a case, one can expect that the determined splitting can be approximated by the weighted average of the strong and the weak exciton lines splittings:

$$\Delta E = \tfrac{3}{4}(E_D - E_A) + \tfrac{1}{4}(E_C - E_B). \qquad \text{(A1)}$$

In Fig. 9(d), the spectra $\mathcal{P}$ and $(\Delta E/2)\mathcal{F}$ are compared. Both strong and weak excitons are split symmetrically with respect to the zero field line. The splitting determined from the $\mathcal{P}$ and $\mathcal{F}$ depths is 12% smaller than $\Delta E_{\mathrm{strong}}$, while it is expected to be 20% smaller according to the weighted average of splittings [Eq. (A1)]. This means that the use of Eq. (A1) results in an underestimation of the $E_D - E_A$ splitting of less than 10%. Several other line shapes were analyzed and for all of them similar result was found. It is worth noting that the effects described in paragraphs (A) and (B) partially compensate one another.

(C) Finally, we checked the applicability of the method in the case when the exciton structures in different polarizations differ in shape (as for $Zn_{1-x}Cr_xTe$, Fig. 6). In Fig. 10, the modeled $\mathcal{P}$ (solid line) and $(\Delta E/2)\mathcal{F}$ (where $\Delta E = 30\ \mathrm{cm}^{-1}$ is the splitting used to model the spectra) are displayed. The blueshifted excitonic components (*A* and *B*) are weaker than these in the other polarization (*C* and *D*) (as in $Zn_{1-x}Cr_xTe$, Fig. 3). The $\mathcal{P}$ spectrum is nonsymmetrical, similarly to the real $Zn_{1-x}Cr_xTe$ spectra (Fig. 6). We note that the minima of calculated $\mathcal{P}$ and $\mathcal{F}$ are shifted one in respect to the other in the same way as in the present experimental situation. To determine the depth of the structures, we used linear interpolation from outside the excitonic structure (Fig. 10). The vertical arrows in the plot show the resulting depth of the structures. The comparison of $\mathcal{P}$ and $\mathcal{F}$ depths yields a splitting which is only 5% larger than the input ΔE value. The above considerations leads to the conclusion that the experimental error of the determined exciton splitting is of the order of 5%, if the spectra for σ^+ and σ^- are similar, as in the case of $Zn_{1-x}Cr_xSe$ and $Zn_{1-x}Cr_xS$, but increases for $Zn_{1-x}Cr_xTe$, since there is a significant difference in shape for the lines in two polarizations and, moreover, the reflectance structure is rather weak (Fig. 5).

[1] *Diluted Magnetic Semiconductors*, edited by J.K. Furdyna and J. Kossut, Semiconductors and Semimetals Vol. 25 (Academic Press, New York, 1988); *Diluted Magnetic Semiconductors*, edited by M. Balkanski and M. Averous (Plenum Press, New York, 1991); J. Kossut and W. Dobrowolski, in *Handbook of Magnetic Materials*, edited by K.H.J. Buschow (North-Holland, Amsterdam, 1993), Vol. 7, p. 231.

[2] K.C. Hass, in *Diluted Magnetic Semiconductors* (Ref. 1).

[3] Su-Huai Wei and A. Zunger, Phys. Rev. B **35**, 2340 (1987); A. Zunger, in *Solid State Physics: Advances in Research and Applications*, edited by F. Seitz and D. Turnbull (Academic Press, New York, 1986), Vol. 39, p. 275.

[4] W. Mac, Nguyen The Khoi, A. Twardowski, J.A. Gaj, and M. Demianiuk, Phys. Rev. Lett. **71**, 2327 (1993).

[5] W. Mac, Nguyen The Khoi, A. Twardowski, and M. Demianiuk, in *Proceedings of 22nd International Conference on Physics of Semiconductors, Vancouver, 1994*, edited by D.J. Lockwood (World Scientific, Singapore, 1994), p. 2573.

[6] W. Mac, Nguyen The Khoi, A. Twardowski, and M. Demianiuk, J. Cryst. Growth **159**, 993 (1995).

[7] J. Blinowski and P. Kacman, Phys. Rev. B **46**, 12 298 (1992); Solid State Commun. **79**, 1021 (1991); Acta Phys. Pol. A **80**, 295 (1991); **82**, 641 (1992); **84**, 693 (1993).

[8] A.K. Bhattacharjee, Phys. Rev. B **46**, 5266 (1992); **49**, 13 987 (1994).

[9] J. Mašek, Solid State Commun. **78**, 351 (1991).

[10] J. Blinowski, P. Kacman, and J.A. Majewski, Acta Phys. Pol. A **88**, 683 (1995); J. Blinowski, P. Kacman, J.A. Majewski, J. Cryst. Growth **159**, 973 (1996).

[11] J.A. Gaj, *Diluted Magnetic Semiconductors* (Ref. 1).

[12] W. Mac, A. Twardowski, P.T.J. Eggenkamp, H.J.M. Swagten, Y. Shapira, and M. Demianiuk, Phys. Rev. B **50**, 14 144 (1994).

[13] D. Heiman, Y. Shapira, and S. Foner, Solid State Commun. **45**, 899 (1983); M. Nawrocki, R. Planel, F. Mollot, and M.J. Kozielski, Phys. Status Solidi B **123**, 99 (1984); D. Heiman, A. Petrou, S.H. Bloom, Y. Shapira, and W. Giriat, Phys. Rev. Lett. **60**, 1876 (1988).

[14] D. Coquillat, J.P. Lascaray, J.A. Gaj, and R. Triboulet, Solid State Commun. **59**, 25 (1986).

[15] H. Venghaus and R. Lambrich, Solid State Commun. **25**, 109 (1978); H. Venghaus, P.E. Simonds, J. Lagois, P.J. Dean, and D. Bimberg, *ibid.* **24**, 5 (1977).

[16] M.E. Lines and J.V. Waszczak, J. Appl. Phys. **48**, 1395 (1977).

[17] V.G. Abrammishvili, S.I. Gubarev, A.V. Komarov, and S.M. Ryabchenko, Fiz. Tverd. Tela **26**, 1095 (1984) [Sov. Phys. Solid State **26**, 666 (1984)].

[18] C. Benoit a la Guillaume, D. Scalbert, and T. Dietl, Phys. Rev. B **46**, 9853 (1992); D. Scalbert, A. Ghazali, and C. Benoit a la Guillaume, *ibid.* **48**, 17 752 (1993); J. Tworzydło, *ibid.* **50**, 14 591 (1994); Solid State Commun. **94**, 10 (1995); **94**, 821 (1995).

[19] A. Twardowski, D. Heiman, M.T. Liu, Y. Shapira, and M. Demianiuk, Phys. Rev. B **53**, 10 728 (1996).

[20] B.E. Larson, K.C. Hass, H. Ehrenreich, and A.E. Carlson, Solid State Commun. **56**, 347 (1985); Phys. Rev. B **37**, 4137 (1988).

[21] J. Kanamori, Prog. Theor. Phys. **30**, 275 (1963).

[22] J.M. Langer and H. Heinrich, Phys. Rev. Lett. **55**, 1414 (1985).